Inhibition of 14q32 microRNA miR-495 reduces lesion formation, intimal hyperplasia and plasma cholesterol levels in experimental restenosis

Sabine M.J. Welten [a, b, 1], Rob C.M. de Jong [a, b, 1], Anouk Wezel [a, e], Margreet R. de Vries [a, b], Martin C. Boonstra [a], Laura Parma [a], J. Wouter Jukema [c], Tetje C. van der Sluis [d], Ramon Arens [d], Ilze Bot [e], Sudhir Agrawal [f], Paul H.A. Quax [a, b, 2], A. Yaël Nossent [a, b, *, 2, 3]

[a] Department of Surgery, Leiden University Medical Center, Leiden, The Netherlands
[b] Einthoven Laboratory for Experimental Vascular Medicine, Leiden University Medical Center, Leiden, The Netherlands
[c] Department of Cardiology, Leiden University Medical Center, Leiden, The Netherlands
[d] Department of Immunohematology and Blood Transfusion, Leiden University Medical Center, Leiden, The Netherlands
[e] Division of Biopharmaceutics, LACDR, Leiden University, Leiden, The Netherlands
[f] Idera Pharmaceuticals, Boston, MA, USA

ARTICLE INFO

ABSTRACT

Background and aims: We aimed at investigating the role of 14q32 microRNAs in intimal hyperplasia and accelerated atherosclerosis; two major contributors to restenosis. Restenosis occurs regularly in patients treated for coronary artery disease and peripheral arterial disease. We have previously shown that inhibition of 14q32 microRNAs leads to increased post-ischemic neovascularization, and microRNA miR-494 also decreased atherosclerosis, while increasing plaque stability. We hypothesized that 14q32 microRNA inhibition has beneficial effects on intimal hyperplasia, as well as accelerated atherosclerosis.
Methods: Non-constrictive cuffs were placed around both femoral arteries of C57BL/6J mice to induce intimal hyperplasia. Accelerated atherosclerotic plaque formation was induced in hypercholesterolemic $ApoE^{-/-}$ mice by placing semi-constrictive collars around both carotid arteries. 14q32 microRNAs miR-329, miR-494 and miR-495 were inhibited in vivo using Gene Silencing Oligonucleotides (GSOs).
Results: GSO-495 administration led to a 32% reduction of intimal hyperplasia. Moreover, the number of macrophages in the arterial wall of mice treated with GSO-495 was reduced by 55%. Inhibition of miR-329 and miR-494 had less profound effects on intimal hyperplasia. GSO-495 administration also decreased atherosclerotic plaque formation by 52% and plaques of GSO-495 treated animals showed a more stable phenotype. Finally, cholesterol levels were also decreased in GSO-495 treated animals, via reduction of the VLDL-fraction.
Conclusions: GSO-495 administration decreased our primary outcomes, namely intimal hyperplasia, and accelerated atherosclerosis. GSO-495 administration also favourably affected multiple secondary outcomes, including macrophage influx, plaque stability and total plasma cholesterol levels. We conclude that 14q32 microRNA miR-495 is a promising target for prevention of restenosis.

1. Introduction

Severe atherosclerosis can cause narrowing and occlusions of affected arteries that require endovascular intervention (such as balloon angioplasty with or without stenting) to restore and maintain blood flow. Unfortunately, vascular damage inflicted by these interventions can lead to rapid restenosis of the artery [1]. Intimal hyperplasia is an important contributor to restenosis, which is characterized by extracellular matrix rearrangements,

* Corresponding author. Department of Surgery, D6-28, Leiden University Medical Center, Albinusdreef 2, 2333 ZA Leiden, The Netherlands.
    E-mail address: a.y.nossent@lumc.nl (A.Y. Nossent).
[1] These authors contributed equally to this work.
[2] These authors contributed equally to this work.
[3] PO Box 9600, 2300 RC Leiden, The Netherlands.

smooth muscle cell (SMC) proliferation and inflammation. On top of that, accelerated atherosclerosis is observed, especially under hypercholesterolemic conditions. Intimal hyperplasia is initiated by damage to the endothelium caused by vascular interventions and results in the activation of endothelial cells (ECs). Subsequently, leukocytes adhere to and infiltrate the vessel wall. These leukocytes secrete inflammatory cytokines and chemokines promoting inflammation, and release matrix metalloproteinases and growth factors leading to extracellular matrix remodelling as well as smooth muscle cell (SMC) proliferation and migration. Accelerated atherosclerosis is initiated by severe flow disturbance combined with the uptake of lipids by macrophages in the vessel wall and subsequent formation of foam cells under hypercholesterolemic conditions.

MicroRNAs are short endogenous RNA molecules which, through binding to the 3′UTR of their target mRNA, regulate gene expression by inhibiting translation of the mRNA into protein. A single microRNA is able to regulate numerous, up to several hundreds, target genes [2]. The fact that a single microRNA can fine-tune the expression of large sets of target genes, and thus genetic programs for specific physiological processes, makes microRNAs an interesting therapeutic tool for complex diseases [3].

We have previously shown that several members of a large microRNA gene cluster on human chromosome 14 (14q32) are highly involved in vascular remodelling, targeting multiple processes important for neovascularization and atherosclerosis [4]. The 14q32 cluster encodes over 54 microRNA genes and is highly conserved in mammals. Inhibition of 14q32 microRNAs miR-329, miR-487b, miR-494 and miR-495 improved post-ischemic neovascularization in a hind limb ischemia model [4]. Inhibition of 14q32 microRNA miR-494 also reduced collar-induced plaque size (accelerated atherosclerosis), increased plaque stability and decreased plasma cholesterol levels [5]. Han et al. also observed upregulation of other 14q32 microRNAs (namely miR-431, miR-668 and miR-758) in atherosclerotic aortas of $ApoE^{-/-}$ mice compared to healthy aortas of C57BL/6 mice [6]. Moreover, hypomethylation of 14q32 microRNAs was observed in human atherosclerotic plaques, resulting in the upregulation of several 14q32 cluster members [7]. The role of 14q32 microRNAs in restenosis however, is unknown.

The involvement of microRNAs in restenosis has been demonstrated in several studies and was recently reviewed [8]. For example, inhibition of miR-21 decreased neointima formation in rat carotid arteries after angioplasty, whereas overexpression of miR-29b inhibited the formation of neointima in balloon-injured rat carotid arteries [9,10]. Based on our previous findings, we hypothesized that 14q32 microRNA inhibition would reduce lesion formation in experimental models for restenosis. In this study, we inhibited 14q32 microRNAs miR-329, miR-494 and miR-495 in a model for intimal hyperplasia and subsequently, we inhibited miR-329 and miR-495 in an accelerated atherosclerosis model and examined the effects on primary outcomes of vascular remodelling or arterial stenosis. In addition, we studied the effects of 14q32 microRNA inhibition on secondary outcomes such as target gene regulation, vascular cell proliferation, plaque stability and cholesterol homeostasis.

2. Materials and methods

2.1. Mice

This study was performed in compliance with the Dutch government guidelines and the Directive 2010/63/EU of the European Parliament. All animal experiments were approved by the Institutional Committee for Animal Welfare of the Leiden University Medical Center (approval reference numbers 13119 and 12165). Male C57BL/6J (10 weeks old) animals were purchased from the Jackson Laboratory. Male $ApoE^{-/-}$ (7—14 weeks old at start of diet) were bred in the local animal breeding facility (Gorlaeus Laboratories, Leiden University, Leiden, the Netherlands). C57BL/6J mice received a chow diet during the whole experiment. $ApoE^{-/-}$ mice were fed a Western-type diet, containing 0.25% cholesterol and 15% cacao butter (Special Diet Services) for six weeks, two weeks prior to surgery. All animals received food and water *ad libitum* during the entire experiment. During surgery, mice were anesthetized by intraperitoneal (i.p) injection of midazolam (8 mg/kg, Roche Diagnostics), medetomidine (0.4 mg/kg, Orion) and fentanyl (0.08 mg/kg, Janssen Pharmaceutica). The adequacy of the anaesthesia was monitored by keeping track of the breathing frequency and the response to toe pinching of the mice. After surgery, mice were antagonized with a subcutaneous injection of flumenazenil (0.5 mg/kg; Fresenius Kabi), antesedan (2.5 mg/kg; AST Pharma) and buprenorphine (0.1 mg/kg; MSD Animal Health).

2.2. Femoral artery cuff mouse model

Intimal hyperplasia was induced by placement of a non-constrictive cuff around the femoral artery of C57BL/6J mice. The left and right femoral arteries were isolated and a rigid, non-constrictive polyethylene cuff was placed around the artery. Thereafter, the wound was closed by a continuous suture. After 21 days, mice were anesthetized and sacrificed via perfusion. Venous blood was drawn in EDTA collection tubes and centrifuged (6000 rpm for 10 min at 4 °C) to obtain plasma. The thorax was opened and mild pressure-perfusion (100 mmHg) with PBS was performed for 4 min by cardiac puncture in the left ventricle. After perfusion with 3.7% formaldehyde, cuffed femoral arteries were harvested, fixed 5 h in formaldehyde and paraffin-embedded.

### 2.3. Carotid collar mouse model

Carotid artery plaque formation was induced by perivascular collar placement as described earlier [11]. In brief, a semi-constrictive cuff collar was placed around both left and right carotid arteries to induce accelerated atherosclerosis (n = 15 per group). Four weeks (28 days) after collar placement, mice were anesthetized and sacrificed via perfusion, after which carotid arteries were harvested, fixed overnight in formaldehyde and paraffin-embedded.

2.4. Gene Silencing Oligonucleotides (GSOs)

Gene Silencing Oligonucleotides (GSOs) were designed with perfect reverse complementarity to the mature target microRNA sequences and synthesized by Idera Pharmaceuticals (GSOs kindly provided by Idera pharmaceuticals). As a negative control, a scrambled sequence was used, designed not to target any known murine microRNA. GSOs consist of two single-stranded 2′O-methylated DNA strands, linked together at their 5'ends by a phosphothioate-linker to avoid TLR-activation [12]. Sequences of microRNAs and GSOs used are given in Supplemental Table 1.

2.5. Uptake of IRDye-800CW labelled GSOs

Two adult male C57BL/6J mice received one non-constrictive cuff around the left femoral artery, while the contra-lateral femoral artery was left unaffected. One day prior to cuff placement, mice were injected intravenously with IRDye-800CW-labelled GSO-329 (0.4 mg/mouse; Idera Pharmaceuticals) or with IRDye-800CW-unlabelled control. Mice were sacrificed by cervical
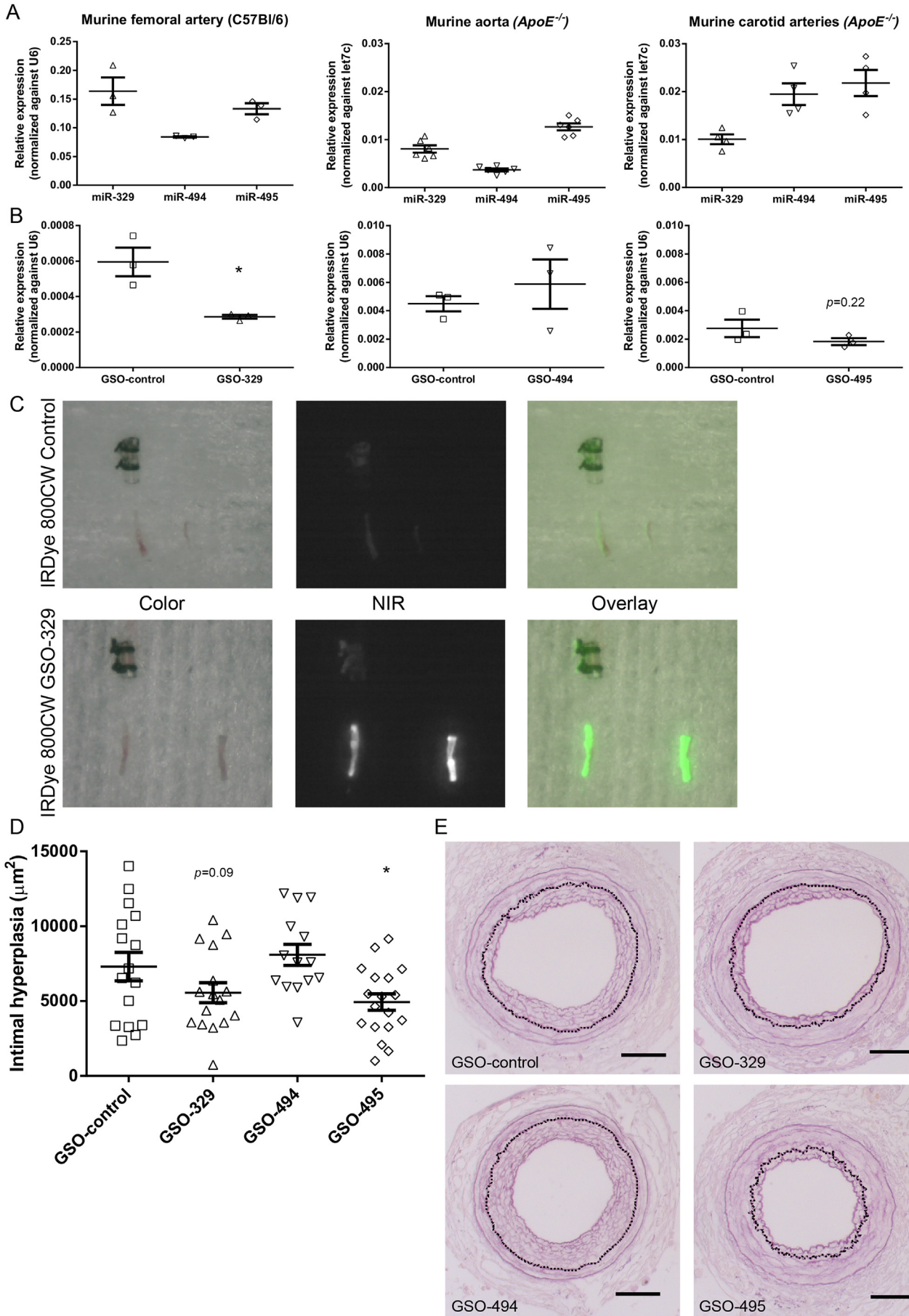
dislocation, 24 h after cuff placement. Near-InfraRed (NIR) fluorescence measurements were performed using the FLARE™ NIR imaging system [13].

2.6. Treatment with GSOs in in vivo models

In case of the femoral artery cuff model, mice received a single intravenous injection of 1 mg GSO dissolved in 200 µl PBS, one day before cuff placement. In case of the carotid collar model, mice received a first intravenous injection of 1 mg GSO dissolved in 200 µl PBS, 4 days after collar placement. At day 18 after collar placement, mice received a second injection of 0.5 mg GSO dissolved in 200 µl PBS.

A subset of mice (n = 3 per group for cuff model and n = 6 per group for collar model) was sacrificed 3 days after the first GSO injection in order to establish downregulation of microRNAs *in vivo*.

2.7. Plasma analysis

Blood was collected from mice prior to surgery, at sacrifice and at indicated timepoints (day 2, day 7, day 21 in cuff model for FACS analysis), by tail bleeding. The concentration of cholesterol in plasma was determined by incubation with 0.025 U/ml cholesterol oxidase (Sigma) and 0.065 U/ml peroxidase and 15 µg/mL cholesterol esterase (Roche Diagnostics) in polyoxyethylene-9-laurylether, and 7.5% methanol. Precipath (standardized serum; Roche Diagnostics) was used as an internal standard. Absorbance was measured at 490 nm.

For lipid profiling, plasma was pooled (n = 5 pooled samples per group, plasma samples of 3 mice were pooled per sample) and diluted 6 times, after which fractionation of plasma lipoproteins was performed using an AKTA-FPLC. Total cholesterol levels were determined in each fraction and in the original pooled sample using a colorimetric assay (Roche Diagnostics, kit 11489232). Absorbance was measured at 490 nm.

2.8. Histology and morphometry

Formaldehyde fixed carotid and femoral arteries were paraffin-embedded and 5 µm thick cross sections of arteries were stained to visualize vessel morphology. Paraffin sections of femoral arteries were stained with Weigert's Elastin to visualize the elastic laminae to determine intimal hyperplasia. Paraffin sections of carotid arteries were stained with hematoxylin-phloxine-saffron (HPS) to determine plaque size. Sirius red staining was used to visualize collagen content.

To visualize macrophages and smooth muscle cells, cross sections of arteries were re-hydrated and endogenous peroxidase activity was blocked. Macrophages and smooth muscle cells were stained using anti-Mac3 (BD Pharmingen, clone M3/84) and anti-smooth muscle actin (SMA; DAKO, clone 1A4) respectively and counterstained using hematoxylin.

To assess proliferation of smooth muscle cells, cross sections of femoral arteries were stained using anti-Ki-67 (proliferation marker) (Abcam, clone SP6) and anti-SMA (DAKO, clone 1A4). Ki-67 was visualized using Alexa 647 conjugated secondary antibody (Invitrogen) and SMA was visualized using Alexa 555 conjugated secondary antibody (Invitrogen). Nuclei were stained using Fluoroshield with DAPI (Sigma).

All quantifications of femoral arteries were performed on six equally spaced cross sections through the cuffed femoral artery by a single blinded observer. Vessel wall parameters, collagen content and smooth muscle cell area were quantified using Qwin (Leica). Macrophage content and the number of Ki-67/SMA positive cells in the cuffed femoral artery of C57Bl6/J mice were counted manually.

Morphometric analysis of carotid arteries was performed on atherosclerotic lesions at the site of maximal stenosis by a single blinded observer. Plaque size, necrotic core, collagen content, smooth muscle cell area and macrophage content were quantified using image analysis software for morphometric analysis (Qwin, Leica).

2.9. Cell culture

Bone marrow (BM) cells isolated from C57BL/6J mice were cultured for 7 days in RPMI medium supplemented with 20% inactivated fetal calf serum (FCSi, PAA), 2 mmol/L L-glutamine (PAA), 100 U/mL penicillin and 100 µg/mL streptomycin and 30% L929 cell-conditioned medium, as the source of macrophage colony-stimulating factor (M-CSF), to generate BM-derived macrophages (BMDMs) [14].

Primary cultured murine vascular smooth muscle cells (vSMC) and cell lines for fibroblasts (3T3) and endothelial cells (H5V) were cultured in complete DMEM GlutaMAX™ medium (Gibco) supplemented with 10% FCSi, 1% penicillin/streptomycin.

VSMCs, H5V and 3T3 cells were plated in triplicate at a density of 10^6 cells/mL. GSOs were added overnight at a concentration of 5 µg/mL, after which the cells were lysed for RNA isolation. For BMDMs, GSOs were added immediately after isolation from BM in a concentration of 5 µg/mL. After three days medium was refreshed with a similar addition of GSOs in a concentration of 5 µg/mL. Four days later, medium was removed and cells were lysed for RNA isolation.

2.10. RNA isolation, cDNA synthesis and quantitative PCR (qPCR)

For measuring basal femoral artery microRNA expression three paraffin embedded femoral artery segments from 21 days after cuff placement were pooled, paraffin was removed using xyleen and tissue was homogenized by grounding using a Pellet Pestle Cordless Motor (Kimble Chase Life Science). For analysis of microRNA inhibition three fresh femoral artery segments from 3 days after cuff placement were pooled and homogenized by grounding using a Pellet Pestle Cordless Motor (Kimble Chase Life Science). Three carotid artery segments from 7 days after collar placement (3 days after GSO injections) were pooled and homogenized using the same

Fig. 1. Expression and inhibition of 14q32 microRNAs miR-329, miR-494 and miR-495, and effects of 14q32 microRNA inhibition on intimal hyperplasia. (A) Relative expression levels (±SEM) of miR-329, miR-494 and miR-495 in the femoral artery of C57BL/6J mice (n = 3 pooled samples, 3 femoral arteries were pooled for 1 sample), the aorta (n = 6) and carotid artery of *ApoE*$^{-/-}$ mice (n = 4 pooled samples, 3 carotids were pooled for 1 sample; data on microRNA expression in *ApoE*$^{-/-}$ mice was adapted with permission from Wezel *et.al.* [5]). (B) Mean expression levels, relative to U6, of miR-329, miR-494 and miR-495 in cuffed femoral arteries (n = 3 pooled samples, 3 femoral arteries were pooled for 1 sample) are shown here 4 days after GSO treatment (±SEM). *p < 0.05. (C) Uptake of IRDye-800CW-labelled GSO-329 in the cuffed femoral artery. In each micrograph the cuffed femoral artery (cuff removed; left) and contra-lateral non-cuffed femoral artery (right) are displayed. Upper panels show femoral arteries of IDRye-800CW-unlabelled control treated animals and lower panels femoral arteries of IRDye-800CW-labelled GSO-329 treated animals, 24 h after cuff placement and 48 h after GSO-injection. Colour images are shown on the left, near-infrared (NIR) images in the middle and an overlay of colour and NIR images is shown on the right. (D) Quantification of intimal hyperplasia 21 days after cuff placement in C57BL/6J mice (n = 14—18 per group) treated with GSOs (±SEM). *p < 0.05 compared to GSO-control. (E) Representative images of elastin staining of cuffed femoral arteries, dashed line represents lamina elastic interna (scale bar = 50 µm). (For interpretation of the references to colour in this figure legend, the reader is referred to the web version of this article.)
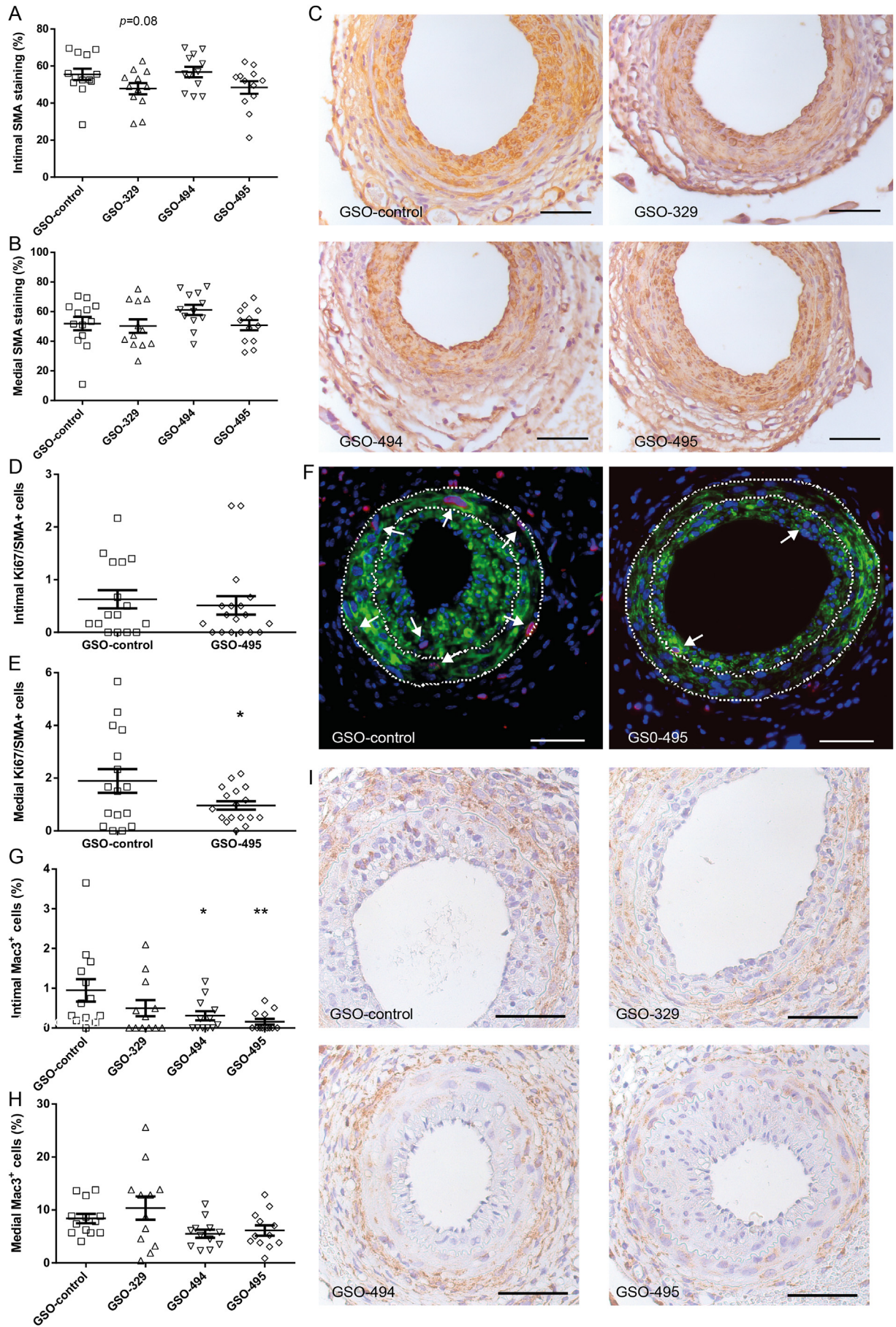
Pellet Pestle Cordless Motor. Liver was isolated and homogenized by grounding with pestle and mortar in liquid nitrogen. Total RNA was extracted using a standard TRIzol-chloroform extraction method. RNA concentration and purity were examined by nanodrop (Nanodrop Technologies). MiR quantification was performed using Taqman® miR assays (Thermo Fisher) following manufacturer's protocol. qPCR was performed on the Viia7 system (Thermo Fisher). Normalization of data was performed using a stably expressed endogenous control (snRNA U6 and mmu-let-7c).

For *in vitro* and *in vivo* experiments, total RNA was extracted from cells and tissues using the standard TRIzol-choloform extraction method. RNA was reverse transcribed using high-capacity RNA to cDNA RT kits (Life technologies) and used for quantitative analysis of mouse genes with the Viia7 system (Applied Biosystems). The relative expression of putative miR-495 target genes was quantified using the QuantiTect SYBR® Green technology (Qiagen). Normalization of the data was performed by using stably expressed endogenous controls (Hprt and Rpl27). Primer sequences can be found in Supplemental Table 2.

2.11. Cholesterol efflux assay

BMDMs, cultured and treated with GSOs as described above, were plated at a density of 0.5×10^6 cells per well. The following day, medium was changed with DMEM containing 10% BSA and 1 μCi/mL ^{3}H-cholesterol (loading medium) to which either GSO-control of GSO-495 was added and cells were treated with 20 mg/mL cholesterol. After 24 h, loading medium was replaced with DMEM with 10% BSA for 1 h. Next, medium was changed for control DMEM with 10% BSA or DMEM with 10% BSA supplemented with HDL (50 μg/mL). After 24 h, radioactivity in the cells and medium was determined by liquid scintillation counting (Packard 1500 Tricard). Cholesterol efflux was defined as ($dpm_{medium}/dpm_{cells} + dpm_{medium}$) x 100% and shown as the percentage of HDL specific efflux, corrected for non-specific efflux to control medium.

2.12. Statistical analysis

Data are expressed as mean ± SEM. Comparisons of absolute miR expression were performed using one-way ANOVA, followed by a Tukey's multiple comparison test. Comparisons of multiple treatment groups with the control group were performed using one-way ANOVA, followed by multiple comparisons without correction for multiple t-tests. Two-tailed Student's t-tests were used to compare a single treatment group with the control group. A level of $p < 0.05$ was considered significant.

3. Results

3.1. In vivo inhibition of miR-329, miR-494 and miR-495 after GSO treatment in the cuff model

Expression levels of 14q32 microRNAs miR-329, miR-494 and miR-495 were measured in the femoral arteries of wildtype C57BL/6J mice and the carotid arteries of *ApoE*$^{-/-}$ mice, representing the two models used to study post-interventional intimal hyperplasia

and accelerated atherosclerosis. Expression of miR-329, miR-494 and miR-495 was also measured in the aorta of *ApoE*$^{-/-}$ mice. In the femoral arteries of wildtype mice, expression of miR-329 and miR-495 was highest, followed by miR-494 expression (Fig. 1A, left panel). As we have previously established, the expression of miR-495 was highest in the aorta of *ApoE*$^{-/-}$ mice (Fig. 1A, middle panel), whereas in the carotid arteries of these animals, both miR-495 and miR-494 were highly expressed (Fig. 1A, right panel) [5].

Next, we measured expression of these microRNAs after GSO treatment in the femoral cuff model. Expression of miR-329, miR-494 and miR-495 was measured at a single timepoint in the femoral artery of in C57BL/6J mice, 3 days after cuff placement, 4 days after GSO injection. MiR-329 was significantly downregulated by 52% in the femoral arteries of C57BL/6J mice compared to GSO-control treated animals. MicroRNA inhibition is a time-dependent process [4] and miR-495 was not downregulated at this specific timepoint. Levels appeared reduced by 34% in the femoral arteries of C57BL/6J mice, but there was no significant difference ($p = 0.22$). For miR-494, we could not observe downregulation at this specific timepoint either (Fig. 1B).

3.2. Uptake of GSOs at site of cuff placement

To visualize uptake of GSOs in the femoral artery, C57BL/6J mice were injected with either IRDye-800CW-labelled GSO-329, or IRDye-800CW-unlabelled control, one day prior to cuff placement. As expression of miR-329 was highest in the femoral artery, we injected mice with IRDye 800CW-labelled GSO-329. Since the GSO chemistry is comparable for GSO-329, GSO-494 and GSO-495, we assume similar uptake of the other GSOs. Uptake of labelled GSO-329 was observed in both cuffed (left) and non-cuffed (right) femoral arteries, whereas minimal uptake was detected in the femoral arteries of mice treated with IRDye-800CW control (Fig. 1C). These data demonstrate effective uptake of GSOs in the femoral arteries. Previously, we have shown that GSOs are also taken up specifically in the carotid arteries of *ApoE*$^{-/-}$ mice, 4 days and 28 days after collar placement [5].

3.3. Effects of miR-329, miR-494 and miR-495 inhibition on vascular remodelling in C57BL/6J mice

At 21 days after cuff placement, intimal hyperplasia was significantly reduced by 33% following treatment with GSO-495 compared to GSO-control. Treatment with GSO-329 resulted in a trend towards decreased intimal hyperplasia by 24% ($p = 0.09$), whereas GSO-494 treatment had no effect on intimal hyperplasia (Fig. 1D and representative images in Fig. 1E). In addition, a decreased intima/media ratio was observed following GSO-495 treatment (35% reduction). This ratio was not decreased in GSO-329 and GSO-494 treated animals (Supplemental Fig. 1A). No differences were found regarding luminal area and lumenstenosis following GSO-494 or GSO-495 treatment (Supplemental Fig. 1B and C). GSO-329 treatment significantly increased luminal area and decreased lumenstenosis in these animals (Supplemental Fig. 1B and C). These data show a beneficial effect of GSO-495 treatment on intimal hyperplasia in C57BL/6J mice.

Fig. 2. Effect of 14q32 microRNA inhibition on vascular smooth muscle cell proliferation and macrophage influx.
Quantification of intimal (A) and medial (B) smooth muscle cell area (%) 21 days after cuff placement in C57BL/6J mice (n = 12–13 per group) treated with GSOs (±SEM). (C) Representative images of SMA staining of cuffed femoral arteries (scale bar = 50 μm). Quantification of intimal (D) and medial (E) smooth muscle cell proliferation 21 days after cuff placement in C57BL/6J mice (n = 16–17 per group) treated with GSO-495 (±SEM). *$p < 0.05$. (F) Representative images of Ki67/SMA staining of cuffed femoral arteries, arrows indicate Ki67/SMA positive cells, dashed lines indicate the elastic laminae (scale bar = 50 μm). Nuclei are shown in blue, SMA staining in green and Ki67 in red.
Quantification of intimal (G) and medial (H) macrophage influx (%) 21 days after cuff placement in C57BL/6J mice (n = 12–13 per group) treated with GSOs (±SEM). *$p < 0.05$, **$p < 0.01$ compared to GSO-control. (I) Representative images of Mac3 staining of cuffed femoral arteries (scale bar = 50 μm). (For interpretation of the references to colour in this figure legend, the reader is referred to the web version of this article.)
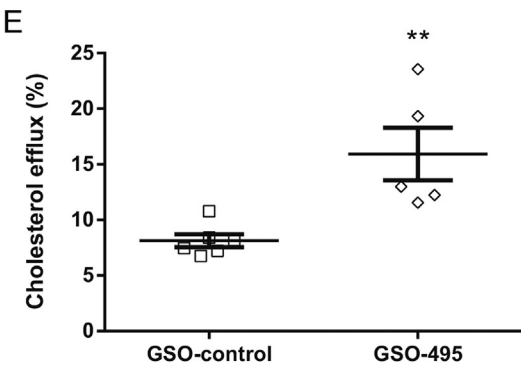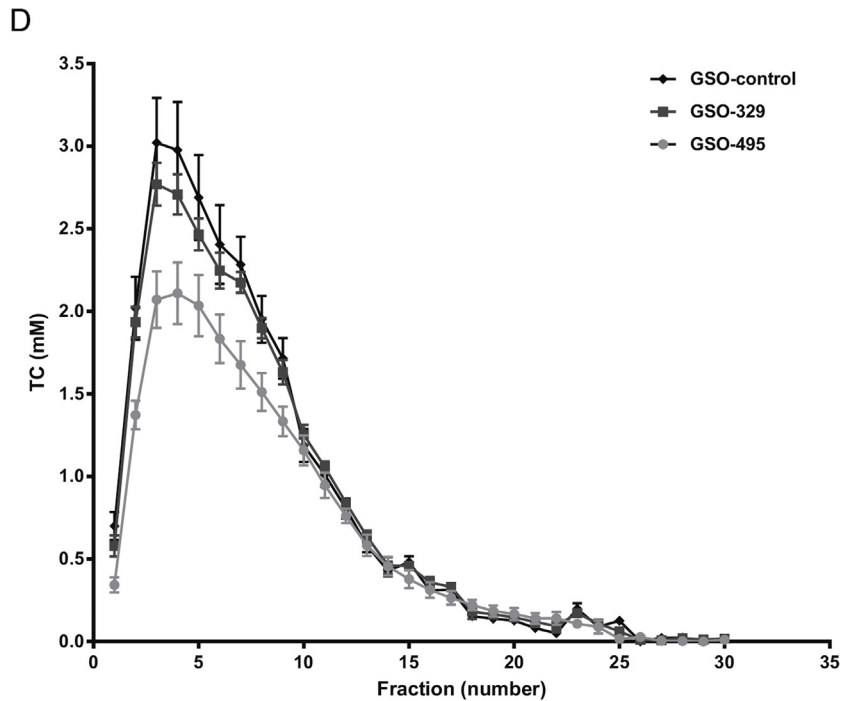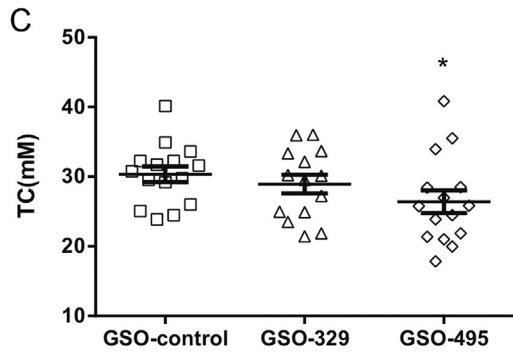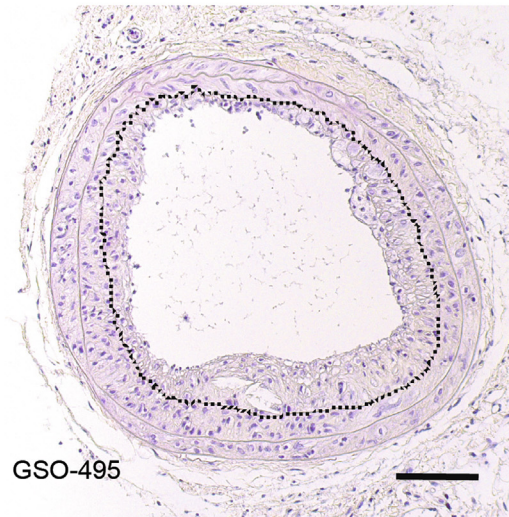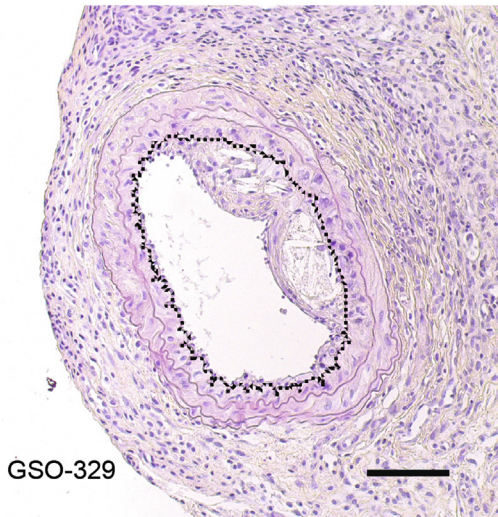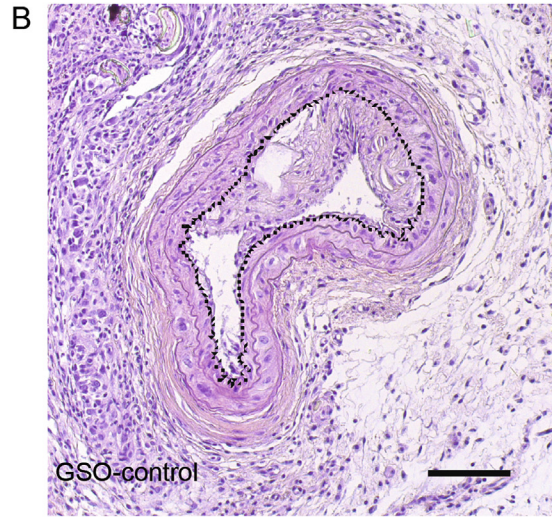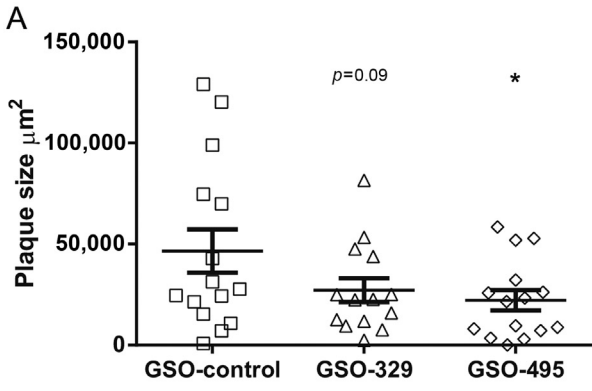
3.4. Effects of miR-329, miR-494 and miR-495 inhibition on vessel wall composition in C57BL/6J mice

To assess the effect of microRNA inhibition on vessel wall composition following cuff placement, we (immuno-)stained serial sections with SMA, Mac-3 or Sirius red. No differences were observed regarding SMC content in the intima and media of GSO treated groups (Fig. 2A and B, representative images in Fig. 2C). Since GSO-495 treatment reduced intimal hyperplasia, we examined the number of proliferating SMCs in this group by staining for Ki67 and SMA and compared the number of double positive cells (Ki67$^+$/SMA$^+$ cells) in GSO-495 treated animals with GSO-control treated animals (Fig. 2D and E). Inhibition of miR-495 reduced the number of proliferating SMCs by 47% in the media of these animals, but not in the intima (Fig. 2D and E, representative images in Fig. 2F).

Following GSO-494 and GSO-495 treatment, macrophage influx was significantly reduced by 35% and 78% respectively in the intimal area compared to GSO-control (Fig. 2G). In the medial area however, macrophage influx was not significantly altered following GSO-494 treatment ($p = 0.13$) or GSO-495 treatment ($p = 0.23$) (Fig. 2H, representative images in Fig. 2I). MicroRNA inhibition did not alter collagen content in either the intima or the media of GSO treated animals (Supplemental Fig. 2A and B, representative images in Supplemental Fig. 2C).

3.5. Effects of miR-495 and miR-329 inhibition in the carotid collar mouse model in ApoE$^{-/-}$ mice

Next, we assessed the effects of 14q32 microRNA miR-329 and miR-495 inhibition on accelerated atherosclerotic plaque formation. Atherosclerotic plaque sizes were significantly decreased with 53% in GSO-495 treated animals (Fig. 3A and representative images in Fig. 3B). In GSO-329 treated animals, a trend towards a 43% decrease in atherosclerotic plaque size compared to GSO-control animals ($p = 0.09$, Fig. 3A, representative images Fig. 3B) was observed. In addition to the decreased plaque size, composition of the lesions was also affected by GSO-495 treatment. Inhibition of miR-495 resulted in smaller necrotic core sizes (60% reduction), whereas inhibition of miR-329 had no significant effects on necrotic core size (Fig. 4A). In addition, the percentage of macrophage content in the lesions was decreased by 30% in GSO-495 treated animals (Fig. 4B), but not in GSO-329 treated animals. No difference was observed in the percentage of SMA positive lesion area between groups (Fig. 4C). Inhibition of miR-495, but not miR-329, increased collagen content by 139% (Fig. 4D), further increasing plaque stability.

Plasma cholesterol levels in GSO-495 treated animals were significantly decreased with 13% (Fig. 3C). Lipid profiling using AKTA-FPLC revealed a reduction in the VLDL fraction after treatment with miR-495 inhibition (Fig. 3D). This reduction in plasma cholesterol and VLDL levels was not observed in animals treated with GSO-329 (Fig. 3C and D). In order to elucidate the mechanism behind the VLDL reduction in GSO-495 treated animals, we investigated the in vitro cholesterol efflux in macrophages. We found that treatment of macrophages with GSO-495 significantly increased cholesterol efflux in vitro by 96% (Fig. 3E).

3.6. Target gene regulation after miR-495 inhibition

We investigated the effects of miR-495 inhibition on target gene regulation. We made a selection of putative target genes that have predicted binding sites for miR-495 in their 3′UTR. Although in vivo inhibition of miR-495 was not statistically significant at this specific timepoint, we could observe upregulation of miR-495 target genes Tgfβ2 and Il13ra1 in the carotid arteries (Fig. 5B). Furthermore, there was a trend towards increased expression of target gene Acvr1 ($p = 0.07$) in the carotids and target gene Il10 was significantly upregulated in the spleen were upregulated in GSO-495 treated animals ($p = 0.05$) (Fig. 5B). In addition, we determined the expression of multiple cholesterol metabolism related target genes of miR-495 in the liver but no differences were observed in the expression of Lrp6, Mttp, Ldlr and Abca1 (Supplemental Fig. 3).

To investigate the effects of miR-495 inhibition on various individual cell types in vascular remodelling, H5V endothelial cells, vSMCs, 3T3 fibroblasts and BMDMs were treated with GSOs against miR-495. Multiple target genes with predicted binding sites for miR-495 were examined, including cytokines, complement components, lipid-related target genes and tissue inhibitors of metalloproteinases (TIMPs). Inhibition of miR-495 led to significant upregulation of Tlr7 in H5V cells and vSMCs ($p = 0.05$), whereas a trend towards upregulation of the anti-inflammatory Il10 was observed in 3T3 cells ($p = 0.06$) and H5V cells ($p = 0.11$) (Supplemental Fig. 4). Other genes that showed a trend towards upregulation after miR-495 inhibition included Cdknb1 ($p = 0.09$) in 3T3 cells, Cd59 ($p = 0.08$) and Ccr2 ($p = 0.06$) in BMDMs.

4. Discussion

Here, we hypothesized that inhibition of 14q32 microRNAs would reduce restenosis through decreased intimal hyperplasia and decreased accelerated atherosclerosis. We show that inhibition of miR-495 leads to less intimal hyperplasia following vascular injury and decreased plaque formation in atherosclerosis prone mice, whilst increasing plaque stability in these animals. In addition, we investigated the effects of 14q32 microRNA miR-495 inhibition on secondary outcomes such as target gene regulation, smooth muscle cell proliferation, plaque stability and cholesterol homeostasis. The 14q32 microRNA gene cluster is the largest known mammalian microRNA gene cluster to date and many 14q32 microRNAs have been implicated within human disease [15]. Recently, we have reported the role of multiple microRNAs from this cluster in several aspects of vascular remodelling, including angiogenesis, arteriogenesis and atherosclerosis [4,5].

MicroRNAs are known for their ability to regulate the expression of numerous genes [16]. Especially miR-495 may have the ability to target a large number of genes; bioinformatics analysis using www.targetscan.org (TargetScan 7.0, consulted January 2016) revealed over 5103 transcripts with in total 7998 putative binding sites for human miR-495 (of which 1015 conserved sites and 6983 poorly conserved sites) and 4879 transcripts with putative binding sites for murine miR-495 (and a total of 7886 sites). It is therefore unlikely that the observed effects are attributable to strong regulation of one target gene in particular, but rather are the sum of modest regulation of multiple target genes involved in all aspects of the processes of vascular remodelling studied here, namely intimal

---

Fig. 3. Effect of 14q32 microRNA miR-495 inhibition on plaque size and cholesterol levels.
(A) Quantification of plaque size 28 days after collar placement in ApoE$^{-/-}$ mice (n = 14—15 per group) treated with GSO-control, GSO-329 or GSO-495. $^*p < 0.05$ compared to GSO-control. (B) Representative images of HPS staining of carotid arteries (scale bar = 100 μm). (C) Total cholesterol levels of ApoE$^{-/-}$ mice treated with GSO-control, GSO-329 or GSO-495, 6 weeks after start of the western type diet. $^*p < 0.05$ compared to GSO-control. (D) Cholesterol profile of GSO treated ApoE$^{-/-}$ mice (n = 5 pooled samples per group, plasma samples of 3 animals were pooled per sample) analysed using AKTA-FPLC. (E) Quantification of cholesterol efflux (%) from macrophages treated with GSO-control or GSO-495. $^{**}p < 0.01$.
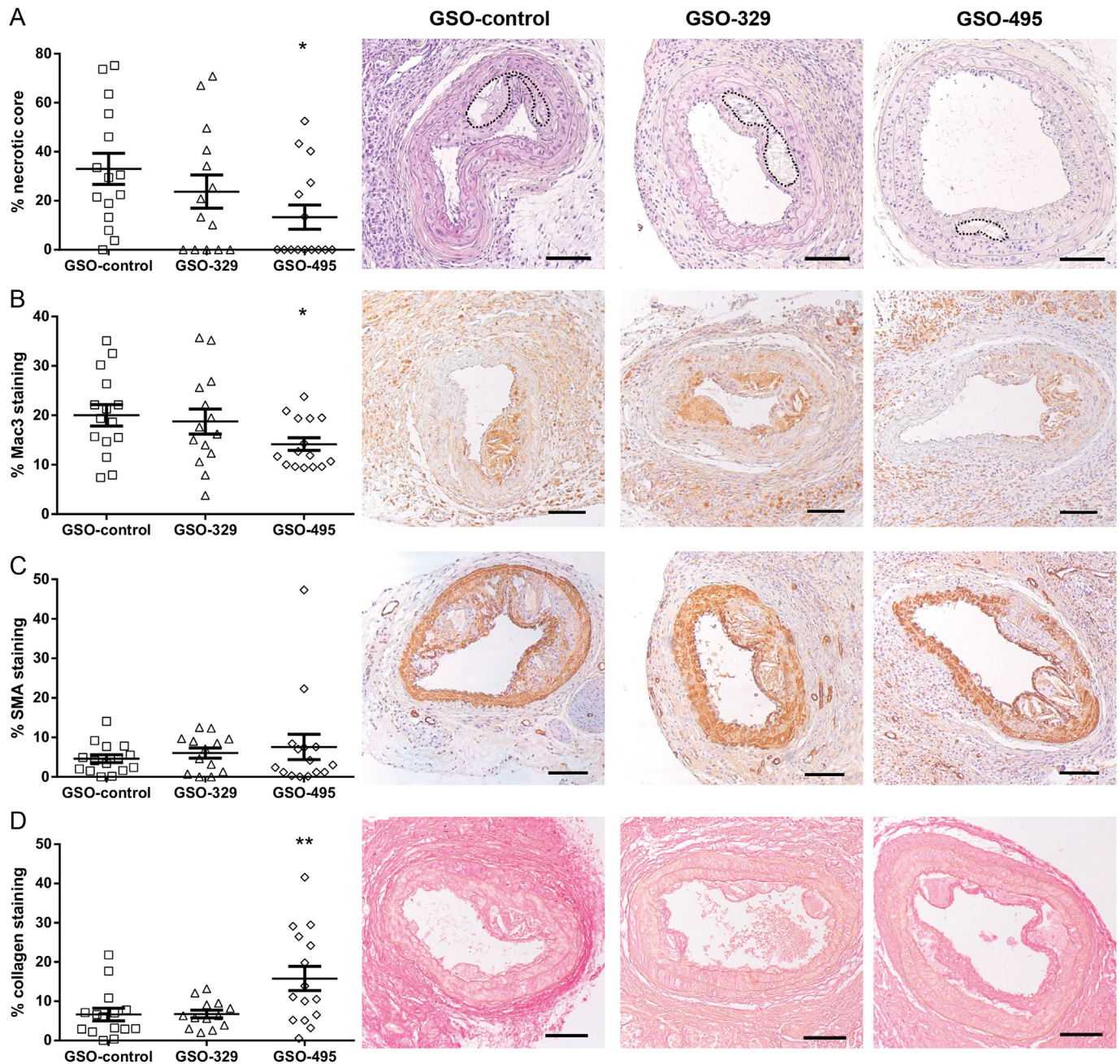
Fig. 4. Effects of 14q32 microRNA miR-495 inhibition on lesion composition 28 days after collar placement in $ApoE^{-/-}$ mice.
(A) Quantification of necrotic core size. (B) Percentage (%) of macrophage influx. (C) Percentage (%) of smooth muscle cell area. (D) Percentage (%) of collagen content. $^*p < 0.05$, $^{**}p < 0.01$ compared to GSO-control. Representative images of (A) HPS staining, (B) Mac3 staining, (C) SMA staining and (D) Sirius red staining are shown (n = 13—15 mice per group, scale bar = 100 μm).

hyperplasia and accelerated atherosclerosis. Moreover, binding of a certain microRNA to its target gene does not completely silence its expression, but rather downtunes its expression [2]. This corresponds to the modest effects that we observed on miR-495 target gene regulation.

In vivo, treatment with GSO-495 led to upregulation of target genes Tgfβ2, Il13ra1 and Il10 and a trend towards upregulation of Acvr1. IL-13, one of the cytokines secreted by CD4$^+$ Th2-cells, inhibits macrophage activation and decreases the production of pro-inflammatory cytokines by activated macrophages [17]. More specifically, the IL-13 receptor alpha 1 chain (Il13ra1) is implicated within the signal transduction route of IL-13 and inhibits interferon-γ induced gene expression in macrophages [18]. We did

observed upregulation of Il10 expression specifically in the spleen following systemic treatment with GSO-495. Since it has been shown that splenic-derived IL-10 has anti-inflammatory properties [19,20], it is plausible that the observed increase in splenic Il-10 expression following GSO-495 has a systemic effect on accelerated atherosclerosis. Likewise, IL-10, which is also a Th2 cytokine has anti-inflammatory properties and protects against atherosclerosis and neointima formation by inhibiting macrophage activation and inhibition of matrix metalloproteinases [21—24]. These findings are in line with our results that GSO-495 treatment decreases macrophage numbers within the arterial lesions investigated. Tgfβ2 is known to be an important regulator of collagen synthesis [25]. This is in line with the observed increase in collagen content and
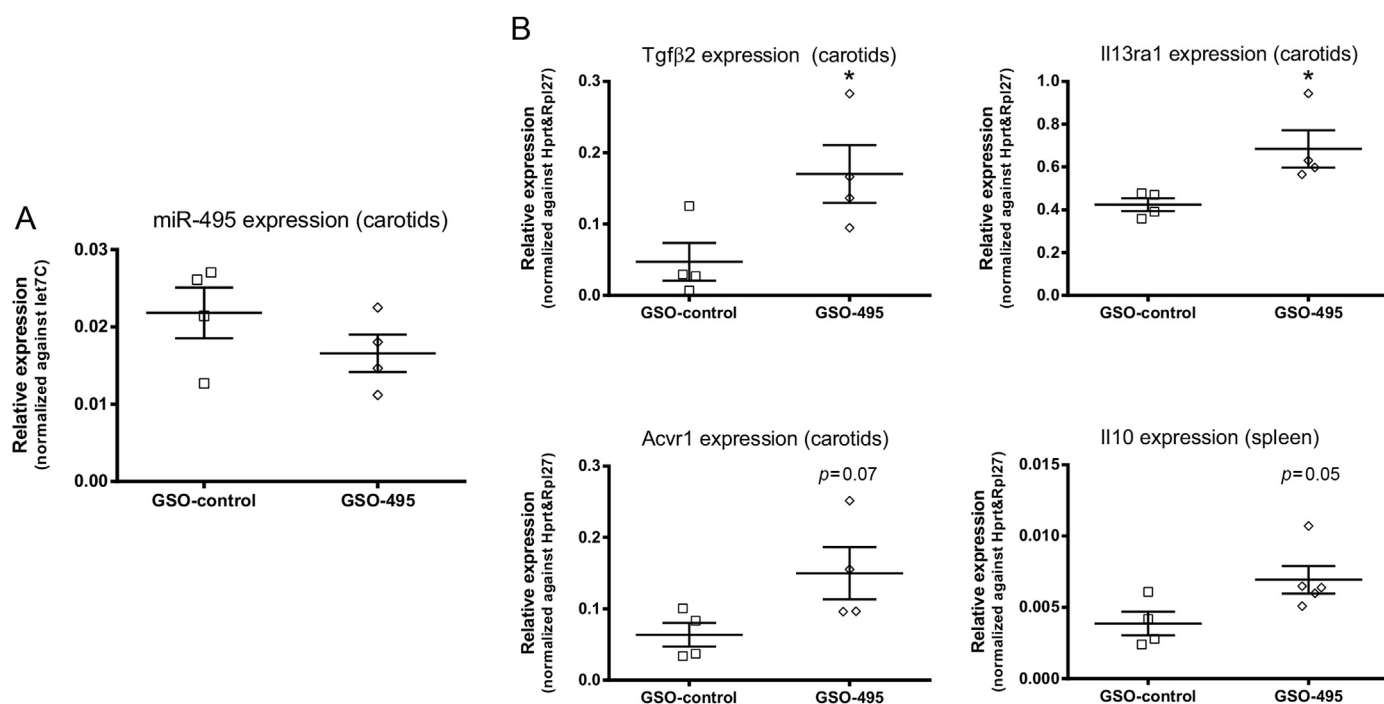
Fig. 5. *In vivo* expression of miR-495 and putative target genes.
(A) Mean expression levels of miR-495 in carotid arteries, relative to let7c, are shown here 3 days after GSO treatment in *ApoE*$^{-/-}$ mice (n = 4 pooled samples per group, 3 carotids were pooled per sample). (B) Mean expression levels of putative miR-495 target genes Tgfβ2, Il13ra1 and Acvr1 in carotids (n = 5 samples per group; 3 carotids were pooled per sample), and Il10 in spleen (n = 5 per group), relative to Hprt and Rpl27, are shown here 3 days after GSO treatment in *ApoE*$^{-/-}$ mice. *$p < 0.05$.

upregulation of Tgfβ2 in the carotid artery. Furthermore, it has been shown that inhibition of Tgfβ1, -β2 and -β3 activity induces atherosclerosis and favours development of an unstable plaque phenotype, which suggests Tgfβ2 has atheroprotective properties and could therefore contribute to the reduced plaque formation seen in this study [26]. Despite the observed upregulation in putative target genes of miR-495, we cannot rule out the possibility that the observed upregulation is the result of an indirect effect of miR-495 inhibition instead of a direct effect of miR-495 inhibition.

Inhibition of miR-495 reduced proliferation of SMCs in neointimal lesions of GSO-495 treated animals. Proliferation and migration of vascular SMCs is one of the most important events in intimal hyperplasia [27]. In agreement with the reduced proliferation of SMCs after miR-495 inhibition, overexpression of miR-495 has previously been shown to increase proliferation of neonatal rat cardiomyocytes [28]. On the other hand, it has also been shown that miR-495 promotes proliferation of HUVECs [29]. These and our findings demonstrate different actions of microRNAs in different cell types, which comes with both benefits and limitations for possible therapeutic uses.

Following GSO-495 treatment, we found a reduction of total cholesterol levels of 13%, which could mainly be attributed to a reduction of VLDL. One of the most frequently used therapy against atherosclerosis is the use of statins, which aims for reduction of (V) LDL cholesterol levels in the blood. Statins reduce (V)LDL cholesterol levels in a range of 40–60% depending on the dose administered, which subsequently reduces the risk of ischemic heart disease by 61% and of stroke by 17% [30]. Although we cannot explain the reduced plaque size and increased stability of the plaques completely by the modest reduction of VLDL plasma cholesterol levels, it is plausible that this reduction contributes, at least partly, to the reduced plaque size and increased plaque stability. This hypothesis is supported by the observed increase in cholesterol efflux from macrophages *in vitro* following GSO-495

treatment. This suggests GSO-495 can inhibit atherogenesis by facilitating removal of cholesterol from the vessel wall to the liver in an HDL dependent manner.

Inhibition of miR-495 also led to a decrease in necrotic core size and macrophage content, while it increased collagen content in atherosclerotic lesions. A decrease in necrotic core size and macrophage content together with an increase in collagen content are characteristics of increased plaque stability [31]. MiR-495 was thus shown to not only contribute to atherosclerotic lesion formation, but also plaque stability in *ApoE*$^{-/-}$ mice. To our knowledge, we are the first to report that inhibition of miR-495 leads to therapeutic benefits in two models of vascular remodelling, namely the femoral artery cuff model for intimal hyperplasia and the carotid collar model for accelerated atherosclerosis. Not only were the lesions in these models reduced in size, but the lesions also contained fewer macrophages and in case of the carotid collar model, plaque stability was increased. Atherosclerosis is the most common underlying cause of cardiovascular disease and can lead to, amongst others, myocardial infarction, ischemic stroke and peripheral arterial disease. Restenosis occurs upon endovascular interventions performed to target these atherosclerotic lesions and involves the re-narrowing of arteries. Reducing both intimal hyperplasia and accelerated atherosclerosis is of crucial importance for the prevention of restenosis.

A limitation of this study is the fact that due to the time-dependent regulation of microRNA expression levels, we cannot attribute all the observed biological effects to miR-495 downregulation with absolute certainty; some of the effects may still be indirect, rather than direct consequences of GSO-495 administration. Future studies should therefore include detailed *in vivo* studies of time-dependent microRNA downregulation and target gene upregulation.

Taken together, however, we conclude that GSO-495 administration improves both primary and secondary parameters of

restenosis. GSO-495 reduces both intimal hyperplasia and accelerated atherosclerosis, which makes miR-495 a highly attractive therapeutic target for patients treated for occlusive arterial disease who are at risk of developing restenosis.

Conflict of interest

Financial support

Author contributions

SMJW, RCMdJ, AW, MRdV, IB, SA, PHAQ and AYN designed the study. SMJW, RCMdJ, AW, MRdV, MCB and TCvdS performed the experiments. SA provided the GSOs. SMJW and RCMdJ wrote the article. IB, MRdV, JWJ, RA, IG, SA, PHAQ and AYN revised the article.

Acknowledgements

Appendix A. Supplementary data

Supplementary data related to this article can be found at http://dx.doi.org/10.1016/j.atherosclerosis.2017.04.011.

References

[1] A.W. Clowes, M.A. Reidy, M.M. Clowes, Mechanisms of stenosis after arterial injury, Lab. Invest. 49 (1983) 208—215.

[2] E. van Rooij, E.N. Olson, MicroRNA therapeutics for cardiovascular disease: opportunities and obstacles, Nat. Rev. Drug Discov. 11 (2012) 860—872.

[3] S.M. Welten, E.A. Goossens, P.H. Quax, A.Y. Nossent, The multifactorial nature of microRNAs in vascular remodelling, Cardiovasc. Res. 110 (2016) 6—22.

[4] S.M. Welten, A.J. Bastiaansen, R.C. de Jong, M.R. de Vries, E.A. Peters, M.C. Boonstra, S.P. Sheikh, N.L. Monica, E.R. Kandimalla, P.H. Quax, A.Y. Nossent, Inhibition of 14q32 MicroRNAs miR-329, miR-487b, miR-494, and miR-495 increases neovascularization and blood flow recovery after ischemia, Circ. Res. 115 (2014) 696—708.

[5] A. Wezel, S.M. Welten, W. Razawy, H.M. Lagraauw, M.R. de Vries, E.A. Goossens, M.C. Boonstra, J.F. Hamming, E.R. Kandimalla, J. Kuiper, P.H. Quax, A.Y. Nossent, I. Bot, Inhibition of MicroRNA-494 reduces carotid artery atherosclerotic lesion development and increases plaque stability, Ann. Surg. 262 (2015) 841—847.

[6] H. Han, Y.H. Wang, G.J. Qu, T.T. Sun, F.Q. Li, W. Jiang, S.S. Luo, Differentiated miRNA expression and validation of signaling pathways in apoE gene knockout mice by cross-verification microarray platform, Exp. Mol. Med. 45 (2013) e13.

[7] E. Aavik, H. Lumivuori, O. Leppanen, T. Wirth, S.K. Hakkinen, J.H. Brasen, U. Beschorner, T. Zeller, M. Braspenning, W. van Criekinge, K. Makinen, S. Yla-Herttuala, Global DNA methylation analysis of human atherosclerotic plaques reveals extensive genomic hypomethylation and reactivation at imprinted locus 14q32 involving induction of a miRNA cluster, Eur. Heart J. 36 (2015) 993—1000.

[8] C. Gareri, S. De Rosa, C. Indolfi, MicroRNAs for restenosis and thrombosis after vascular injury, Circ. Res. 118 (2016) 1170—1184.

[9] R. Ji, Y. Cheng, J. Yue, J. Yang, X. Liu, H. Chen, D.B. Dean, C. Zhang, MicroRNA expression signature and antisense-mediated depletion reveal an essential role of MicroRNA in vascular neointimal lesion formation, Circ. Res. 100 (2007) 1579—1588.

[10] J. Lee, S. Lim, B.W. Song, M.J. Cha, O. Ham, S.Y. Lee, C. Lee, J.H. Park, Y. Bae, H.H. Seo, M. Seung, E. Choi, K.C. Hwang, MicroRNA-29b inhibits migration and proliferation of vascular smooth muscle cells in neointimal formation, J. Cell Biochem. 116 (2014) 598—608.

[11] J.H. von der Thusen, T.J. van Berkel, E.A. Biessen, Induction of rapid atherogenesis by perivascular carotid collar placement in apolipoprotein E-deficient and low-density lipoprotein receptor-deficient mice, Circulation 103 (2001) 1164—1170.

[12] L. Bhagat, M.R. Putta, D. Wang, D. Yu, T. Lan, W. Jiang, Z. Sun, H. Wang, J.X. Tang, N. La Monica, E.R. Kandimalla, S. Agrawal, Novel oligonucleotides containing two 3'-ends complementary to target mRNA show optimal gene-silencing activity, J. Med. Chem. 54 (2011) 3027—3036.

[13] S.L. Troyan, V. Kianzad, S.L. Gibbs-Strauss, S. Gioux, A. Matsui, R. Oketokoun, L. Ngo, A. Khamene, F. Azar, J.V. Frangioni, The FLARE intraoperative near-infrared fluorescence imaging system: a first-in-human clinical trial in breast cancer sentinel lymph node mapping, Ann. Surg. Oncol. 16 (2009) 2943—2952.

[14] Y. Zhao, M. Pennings, R.B. Hildebrand, D. Ye, L. Calpe-Berdiel, R. Out, M. Kjerrulf, E. Hurt-Camejo, A.K. Groen, M. Hoekstra, W. Jessup, G. Chimini, T.J. van Berkel, M. Van Eck, Enhanced foam cell formation, atherosclerotic lesion development, and inflammation by combined deletion of ABCA1 and SR-BI in Bone marrow-derived cells in LDL receptor knockout mice on western-type diet, Circ. Res. 107 (2010) e20—e31.

[15] L. Benetatos, E. Hatzimichael, E. Londin, G. Vartholomatos, P. Loher, I. Rigoutsos, E. Briasoulis, The microRNAs within the DLK1-DIO3 genomic region: involvement in disease pathogenesis, Cell Mol. Life Sci. 70 (2013) 795—814.

[16] N. Rajewsky, microRNA target predictions in animals, Nat. Genet. 38 Suppl (2006) S8—S13.

[17] T.M. Doherty, R. Kastelein, S. Menon, S. Andrade, R.L. Coffman, Modulation of murine macrophage function by IL-13, J. Immunol. 151 (1993) 7151—7160.

[18] F. Sheikh, H. Dickensheets, J. Pedras-Vasconcelos, T. Ramalingam, L. Helming, S. Gordon, R.P. Donnelly, The Interleukin-13 receptor-alpha1 chain is essential for induction of the alternative macrophage activation pathway by IL-13 but not IL-4, J. Innate. Immun. 7 (2015) 494—505.

[19] K. Gotoh, M. Inoue, T. Masaki, S. Chiba, T. Shimasaki, H. Ando, K. Fujiwara, I. Katsuragi, T. Kakuma, M. Seike, T. Sakata, H. Yoshimatsu, A novel anti-inflammatory role for spleen-derived interleukin-10 in obesity-induced inflammation in white adipose tissue and liver, Diabetes 61 (2012) 1994—2003.

[20] K. Gotoh, M. Inoue, T. Masaki, S. Chiba, T. Shimasaki, H. Ando, K. Fujiwara, I. Katsuragi, T. Kakuma, M. Seike, T. Sakata, H. Yoshimatsu, A novel anti-inflammatory role for spleen-derived interleukin-10 in obesity-induced hypothalamic inflammation, J. Neurochem. 120 (2012) 752—764.

[21] Z. Mallat, S. Besnard, M. Duriez, V. Deleuze, F. Emmanuel, M.F. Bureau, F. Soubrier, B. Esposito, H. Duez, C. Fievet, B. Staels, N. Duverger, D. Scherman, A. Tedgui, Protective role of interleukin-10 in atherosclerosis, Circ. Res. 85 (1999) e17—e24.

[22] K.B. Holven, B. Halvorsen, V. Bjerkeli, J.K. Damas, K. Retterstol, L. Morkrid, L. Ose, P. Aukrust, M.S. Nenseter, Impaired inhibitory effect of interleukin-10 on the balance between matrix metalloproteinase-9 and its inhibitor in mononuclear cells from hyperhomocysteinemic subjects, Stroke 37 (2006) 1731—1736.

[23] P. Wang, P. Wu, M.I. Siegel, R.W. Egan, M.M. Billah, Interleukin (IL)-10 inhibits nuclear factor kappa B (NF kappa B) activation in human monocytes. IL-10 and IL-4 suppress cytokine synthesis by different mechanisms, J. Biol. Chem. 270 (1995) 9558—9563.

[24] D. Eefting, A. Schepers, M.R. de Vries, N.M. Pires, J.M. Grimbergen, T. Lagerweij, L.M. Nagelkerken, P.S. Monraats, J.W. Jukema, J.H. van Bockel, P.H. Quax, The effect of interleukin-10 knock-out and overexpression on neointima formation in hypercholesterolemic APOE*3-Leiden mice, Atherosclerosis 193 (2007) 335—342.

[25] X. Wang, P. Smith, L.L. Pu, Y.J. Kim, F. Ko, M.C. Robson, Exogenous transforming growth factor beta(2) modulates collagen I and collagen III synthesis in proliferative scar xenografts in nude rats, J. Surg. Res. 87 (1999) 194—200.

[26] Z. Mallat, A. Gojova, C. Marchiol-Fournigault, B. Esposito, C. Kamate, R. Merval, D. Fradelizi, A. Tedgui, Inhibition of transforming growth factor-beta signaling accelerates atherosclerosis and induces an unstable plaque phenotype in mice, Circ. Res. 89 (2001) 930—934.

[27] A.C. Newby, A.B. Zaltsman, Molecular mechanisms in intimal hyperplasia, J. Pathol. 190 (2000) 300—309.

[28] A.L. Clark, F.J. Naya, MicroRNAs in the myocyte enhancer factor 2 (MEF2)-regulated Gtl2-Dio3 noncoding RNA locus promote cardiomyocyte proliferation by targeting the transcriptional coactivator Cited2, J. Biol. Chem. 290 (2015) 23162—23172.

[29] D. Liu, X.L. Zhang, C.H. Yan, Y. Li, X.X. Tian, N. Zhu, J.J. Rong, C.F. Peng, Y.L. Han, MicroRNA-495 regulates the proliferation and apoptosis of human umbilical vein endothelial cells by targeting chemokine CCL2, Thromb. Res. 135 (2015) 146—154.

[30] M.R. Law, N.J. Wald, A.R. Rudnicka, Quantifying effect of statins on low density lipoprotein cholesterol, ischaemic heart disease, and stroke: systematic review and meta-analysis, BMJ 326 (2003) 1423.

[31] G.K. Hansson, P. Libby, I. Tabas, Inflammation and plaque vulnerability, J. Intern. Med. 278 (2015) 483—493.